

## Ultrafast hot-carrier relaxation in silicon monitored by phase-resolved transient absorption spectroscopy

Martin Wörle,<sup>1</sup> Alexander W. Holleitner <sup>1,2</sup> Reinhard Kienberger <sup>1</sup> and Hristo Iglev <sup>1,\*</sup>

<sup>1</sup>Physik-Department, Technische Universität München, James-Frank-Straße 1, 85748 Garching, Germany

<sup>2</sup>Munich Center for Quantum Science and Technology (MCQST), Schellingstrasse 4, 80799 München, Germany



(Received 24 November 2020; revised 21 May 2021; accepted 25 May 2021; published 12 July 2021)

The relaxation dynamics of hot carriers in silicon (100) is studied via a holistic approach based on phase-resolved transient absorption spectroscopy with few-cycle optical pulses. After excitation by a sub-5-fs light pulse, strong electron-electron coupling leads to an ultrafast single electron momentum relaxation time of 10 fs. The thermalization of the hot carriers is visible in the temporal evolution of the effective mass and the collision time as extracted from the Drude model. The optical effective mass decreases from  $0.3m_e$  to about  $0.125m_e$  with a time constants of 58 fs, while the collision time increases from 3 fs for the shortest timescales with a saturation at approximately 18 fs with a time constant of 150 fs. The observation shows that both Drude parameters exhibit different dependences on the carrier temperature. The presented information on the electron mass dynamics as well as the momentum-, and electron-phonon scattering times with unprecedented time resolution is important for all hot-carrier optoelectronic devices.

DOI: [10.1103/PhysRevB.104.L041201](https://doi.org/10.1103/PhysRevB.104.L041201)

Ultrafast scattering of highly energetic (hot) carriers in semiconductors plays crucial role in nanoscale semiconductor junctions [1], hot-carrier solar cells [2–4] and next-generation thermo- and optoelectronics [5,6]. The rapid development of time-resolved spectroscopy enables a direct monitoring of the scattering dynamics. In particular, time- and angle-resolved photoemission spectroscopy gives experimental information on the electron momentum and energy relaxation [7,8], while femtosecond THz spectroscopy is sensitive to hot-electron transport properties and to free-carrier plasma effects [9–11]. Furthermore, attosecond extreme ultraviolet (XUV) transient spectroscopy enables the access to the ultrafast dynamic of inter-band electron relaxation processes [12–14]. Despite accumulating knowledge, a clear understanding of the ultrafast scattering processes of hot electrons even in the conduction band of silicon (Si) is still incomplete, although it is the most fundamental semiconductor with significant importance for the microelectronic industry.

Recent progress in theoretical calculations from first principles has made it possible to gain a deeper insight into the electron relaxation dynamics in Si. The calculations show that the momentum scattering time due to electron-phonon coupling is supposed to be shorter than 10 fs for excess energies above 1.5 eV, although the value is one order of magnitude shorter than experimentally reported ones [8]. The concept of quasiequilibrated hot-electron ensemble indicates that the transient relaxation of hot electrons is governed by two relaxation times with different magnitude: the momentum relaxation time and the energy relaxation time [7,8]. Generally, the relaxation dynamics of the hot-carrier ensemble can be analyzed in terms of an elevated carrier temperature, which

decays with the characteristic electron-phonon scattering time [15–17]. Transient reflective measurements and femtosecond THz spectroscopy on Si proved to be a powerful tool for monitoring Drude-response and related parameters, like effective carrier masses and collision times [9,15,16,18] as well as electron-electron [10] and electron-phonon interactions [11,19–21]. However, some of these experiments overestimate the extracted time constants due to limited time-resolution.

In this letter we report a peculiar phase-resolved transient absorption scheme with few-cycle pump and probe pulses. The comprehensive ansatz, with simultaneous detection of pump-induced absorption and refractive index changes, reveals a full picture of the ultrafast free carrier relaxation in Si, including the single electron momentum relaxation time, electron-phonon scattering time, transient effective carrier mass, and Drude collision time. The gained results could be important for novel application in electronics like energy storage [22], ultrafast electro-optical modulation techniques [23,24], and signal processing [25].

The principle of the current experiment is schematically shown in Fig. 1. A collinear beam geometry at the sample was chosen to achieve the best possible temporal resolution [Fig. 1(a)]. The optical excitation is achieved by sub-5 fs pulses at 750 nm, while the transient relaxation dynamics are monitored in the spectral range between 1250 and 1950 nm [26–28]. To get access to the pump introduced refractive index change the probe pulse is split into two copropagating pulses (probe and reference). The temporal sequence of the used reference, pump and probe pulses is indicated in Fig. 1(b) (for more details on the experiment see the Supplemental Material (SM) [29]). The energy transmittance  $T$  of the probing pulse through the excited sample is measured for parallel ( $\parallel$ ) and perpendicular ( $\perp$ ) polarizations relative to the polarization plane of the pump and compared with the probe

\*hristo.iglev@ph.tum.de

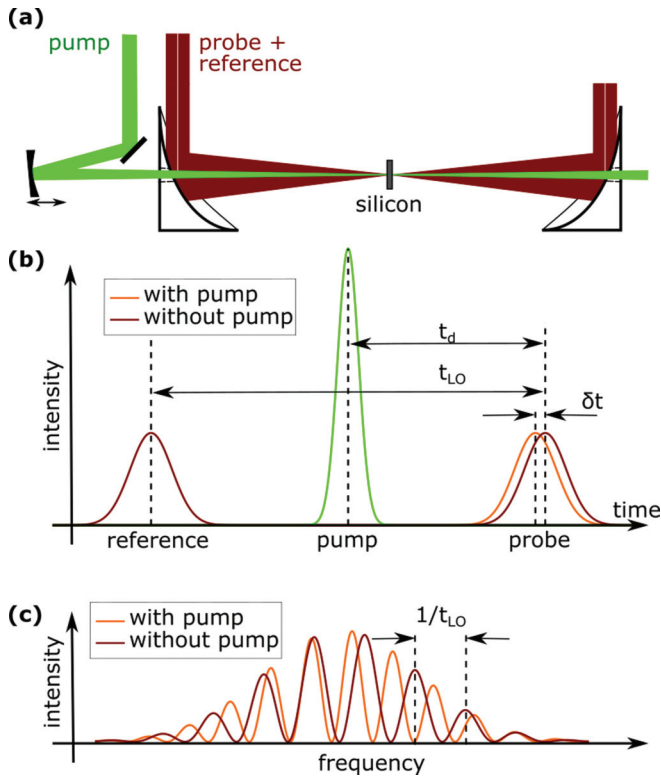


FIG. 1. (a) Schematic representation of the collinear sample layout. (b) Scheme of the used pulse sequence. The pump induced refractive index change causes a temporal shift of  $\delta t$ . (c) Schematics of the interference pattern measured by the IR detection system for both situations with and without excitation.

transmittance  $T_0$  for blocked excitation beam. In this way, the induced change of the optical density,  $\Delta OD_{\parallel,\perp} = -\log(T_{\parallel,\perp}/T_0)$  is determined for various probe wavelengths  $\lambda$  and delay times  $t_d$ . These transient absorption measurements are performed with a blocked reference pulse.

The overlap of probe and reference beams on the infrared (IR) detector arrays leads to an interference pattern, which is schematically shown in Fig. 1(c). The frequency spacing between two neighboring maxima is inverse proportional to the reference-probe delay time ( $\Delta\nu = 1/t_{LO}$ ), while the exact frequency position of the interference fringes depends on their relative phase shift. The photogenerated electrons and holes in the Si sample will change its refractive index  $\Delta n$ , indicated by the additional temporal shift  $\delta t = \Delta n \times L/c$  in Fig. 1(b). Here  $L$  is the sample thickness and  $c$  denotes the speed of the light. Thus,  $\Delta n$  causes a phase shift of the subsequent probe pulse relative to the reference pulse. Note that the reference passes through an unexcited sample, which implicates  $t_d < t_{LO}$ . The pump-induced phase shift  $\Delta\Phi$  is extracted via Fourier-transform spectral interferometry [30,31]. In order to improve the signal-to-noise ratio, the spectrum measured with probe and reference beams is subtracted by the spectrum taken for blocked reference. The gained pure interference signal is converted from wavelength into frequency domain and Fourier transformed. The obtained peak at  $1/t_{LO}$  is shifted to 0. The inverse Fourier transformation yields the phase difference between probe and reference. This procedure

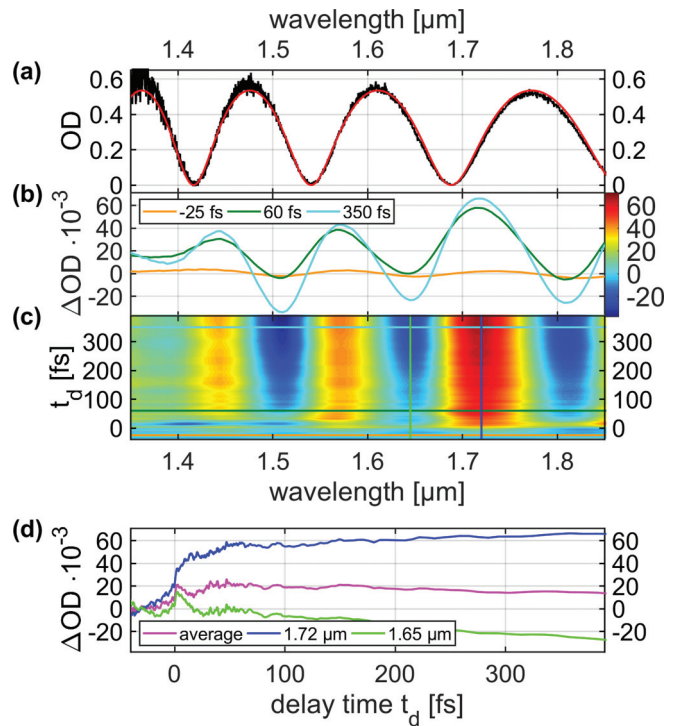


FIG. 2. (a) FTIR absorption spectra of a  $2.5 \mu\text{m}$  thick Si (100) sample (experimental data in black, theory in red). (b) Isotropic transient absorption spectra measured at three selected delay times (see inset). (c) The full data set presented as a 2D color plot with color scale given next to (b). (d) Signal transients measured at  $1.65 \mu\text{m}$  and  $1.72 \mu\text{m}$ , together with the signal averaged over the spectral range from  $1.39$  to  $1.81 \mu\text{m}$ .

is repeated at every delay time  $t_d$  for open and for blocked pump beam. The difference of the last two values provides the pump-induced phase shift  $\Delta\Phi$ . Note that the phase-resolved measurements required sufficient modulation depth which additionally reduces the detectable spectral range to  $1.35$ – $1.85 \mu\text{m}$ .

We emphasize, that the transient amplitude and phase changes yielded by this technique provide the full information of the pump-induced changes in the subsequent probing pulse [30,31]. Thus, the current method is comparable to the time-resolved THz spectroscopy [9–11].

The investigated sample is a monocrystalline (100) silicon (Si) plate with a thickness  $L \approx 2.5 \mu\text{m}$ . The small sample thickness allows us to overcome the limitations in the temporal resolution caused by the different group velocities of pump and probe pulses. However, the large refractive index of Si ( $n_0 \approx 3.5$ ) leads to significant surface reflection of the probe radiation, which causes the thin sample plate to act as a Fabry-Pérot interferometer (FPI). The measured steady-state Fourier transform infrared (FTIR) absorption of the Si plate is shown in Fig. 2(a) (black line). The cavity finesse extracted from the observed spectral modulations of  $2.46$  [32] is in excellent agreement with the expected surface reflection of  $0.3$  [see red fitted line in Fig. 2(a)]. It should be noted that averaging the steady-state spectrum over the free spectral range ( $\Delta\nu_{\text{FSR}} = 2Ln_0/c$ ) of the FPI equals the sum of the individual

attenuations of both cavity mirrors (i.e.,  $\bar{A} = -2 \log_{10}(1-R)$ , for more details see Fig. S2 in the SM [29]).

The optical excitation by sub-5 fs pulses at 750 nm and pulse energy of 1.8  $\mu\text{J}$  leads to generation of free carriers with significant absorption in the near infrared spectral range. The isotropic changes of the optical density ( $\Delta OD_{\text{iso}} = (\Delta OD_{\parallel} + 2\Delta OD_{\perp})/3$ ) measured in the thin Si plate are shown in Figs. 2(b) and 2(c). The transient spectra show sinusoidal modulations with positive and negative absorption values, which are caused by Fabry-Pérot interference in the sample [red line in Fig. 2(a)]. The particular modulations are not observed for a 2-mm-thick Si sample (see Fig. S3 in the SM [29]). Most interestingly, the modulations measured for longer delay times [cyan line in Fig. 2(b)] are off-phase compared to the steady-state spectrum shown in Fig. 2(a). These observations give evidence for simultaneous pump-induced absorption and refractive index changes in the excited Si sample.

Averaging of the absorption data over a spectral range proportional to  $\Delta v_{\text{FSR}}$  facilitates the extraction of the pure excited state population dynamics (see Fig. S4 in the SM [29]). The transient data averaged over the spectral range from 1.39 to 1.81  $\mu\text{m}$  ( $\approx 3 \times \Delta v_{\text{FSR}}$ ) are shown in Fig. 2(d) (magenta), together with the transients measured at 1.65 and 1.72  $\mu\text{m}$ . The figure indicates fast relaxation dynamics in the first 50 fs, followed by a slower signal increase in the next 500 fs. In general, the data measured in the absorption maximum at 1.72  $\mu\text{m}$  shows similar temporal dynamics as the averaged signal, but at higher signal-to-noise ratio. This can be expected for samples with small spectral dynamics in the monitored spectral range.

Figure 3 presents the measured pump-induced isotropic phase shifts  $\Delta \Phi_{\text{iso}} = (\Delta \Phi_{\parallel} + 2\Delta \Phi_{\perp})/3$ , which reflects the transient change of the refractive index  $\Delta n$ . We emphasize that the data shown in Figs. 2 and 3 provide that the measured signals are in accordance with the expected negative  $\Delta n$  values for free electrons. The time-resolved data show in-phase spectral modulation compared to the steady-state absorption [see Fig. 2(a)], however, their relative modulation depth is much smaller than in the transient absorption signal [cf. Fig. 2(b)]. The transient phase shift shows an ultrafast initial signal change, which is followed by significant amplitude increase within the first 200 fs [see Figs. 3(b) and 3(c)].

The main physical effects responsible for the change in the linear optical properties of strongly excited silicon are state and band filling, band-structure renormalization, and free-carrier response [18]. Note that the lattice heating responsible for the band-gap narrowing occurs on time scales of 10 ps, while the change due to band filling can be neglected for carrier densities in the order of  $10^{19} \text{ cm}^{-3}$ , as estimated for the present experiment. Thus the optical properties within the first few 100 fs are very likely governed by the free-carrier response [33]. Optical-pump THz-probe spectroscopy on various electron systems has demonstrated the applicability of the Drude model to deduce information on the transient conductivity [34–36]. Time-dependent density functional theory calculation on the dielectric response of crystalline SI to high-intense laser irradiation show that the Drude model can be used to describe the transient dielectric response if the carrier collision time and the effective carrier mass depends on the

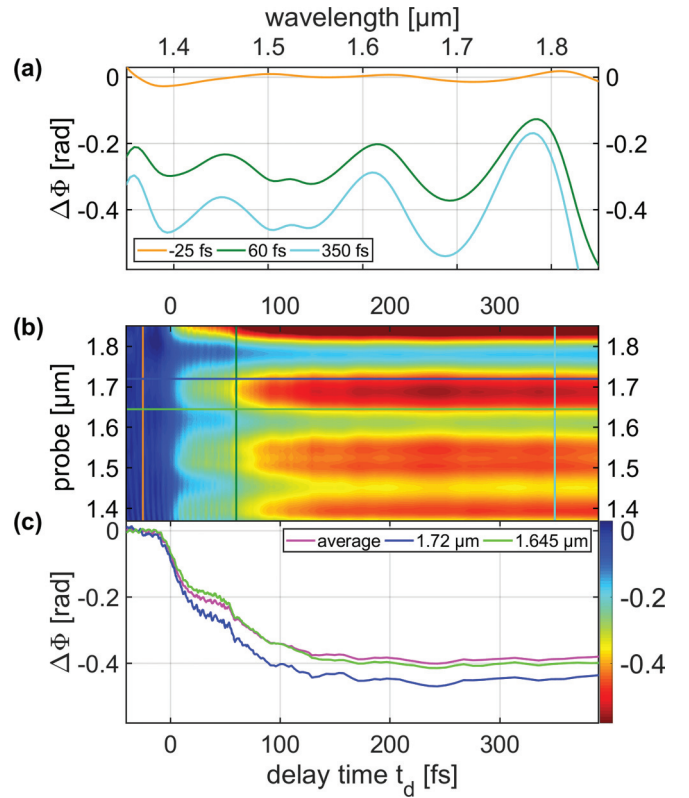


FIG. 3. Transient isotropic phase changes  $\Delta \Phi_{\text{iso}}$  in Si after excitation with few-cycle laser pulse. (a) Phase changes measured at three selected delay times (see inset). (b) The full data set presented as a 2D color plot with color scale given next to (c). (c) Data measured at 1.645 and 1.72  $\mu\text{m}$ , together with the signal averaged over the spectral range from 1.39 to 1.81  $\mu\text{m}$ .

carrier temperature [17]. Assuming the validity of the Drude model also in the high-field regime of the present work with a plasma frequency much higher than the characteristic lattice frequencies, the complex refractive index can be written as [18,33]

$$\Delta \tilde{n} = \left( \frac{e^2 N_{e-h}}{\epsilon_0 m_{\text{opt}}^*} \right) \frac{1}{\omega^2 + i\omega/\tau_c}, \quad (1)$$

with the unperturbed refractive index  $n_0$ , electron charge  $e$ , density of photogenerated electron-hole pairs  $N_{e-h}$ , vacuum permittivity  $\epsilon_0$ , optical effective mass of the charge carriers  $m_{\text{opt}}^*$ , central probe frequency  $\omega$ , collision time  $\tau_c$ , and plasma frequency  $\omega_p = (e^2 N_{e-h} / \epsilon_0 m_{\text{opt}}^*)^{1/2}$ . By linking the real and imaginary parts of Eq. (1) with the measured variables one gets

$$\Delta \Phi = \frac{\pi L}{n_0 \lambda} \times \frac{\omega_p^2}{\omega^2 + 1/\tau_c^2}, \quad (2)$$

$$\Delta OD = \frac{2\pi L}{n_0 \lambda \ln 10} \times \frac{\omega_p^2}{\omega \tau_c (\omega^2 + 1/\tau_c^2)}. \quad (3)$$

From Eqs. (2) and (3) the collision time can be extracted to

$$\tau_c = \frac{2|\Delta \Phi|}{\omega \Delta OD \ln 10}. \quad (4)$$

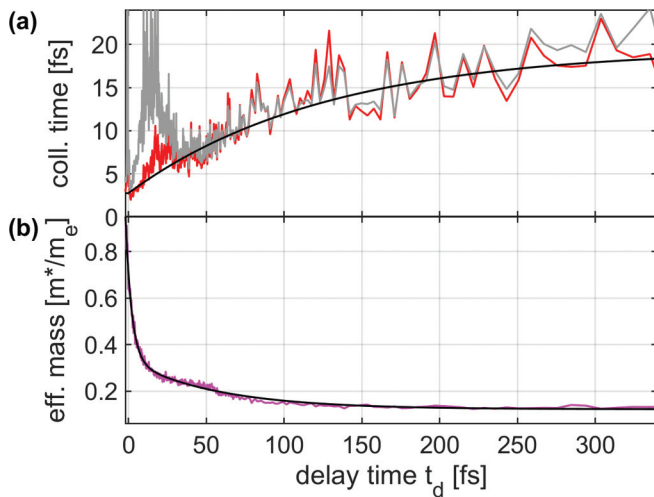


FIG. 4. (a) Collision time for probe polarization parallel (red) and perpendicular (gray) relative to the pump polarization. Calculated black line representing an exponential fit with a time constant of  $150 \pm 30$  fs. (b) Reduced effective mass of the charge carriers extracted from the spectral averaged experimental data (magenta). The black line represents a biexponential fit with time constants of 4 and 58 fs.

Assuming a constant carrier concentration on the sub-picosecond time scale, the electron-hole pair concentration can be estimated from the averaged absorption data [see magenta line in Fig. 2(c),  $\Delta OD \approx 0.016$  for  $t_d = 250$  fs] and the reported electron-hole pair absorption cross section  $\sigma_{e-h} \approx 9.4 \times 10^{-18}$  cm<sup>2</sup> for a central wavelength of  $1.6 \mu\text{m}$  [37]. The extracted electron-hole pair concentration is  $N_{e-h} = (\ln 10 \times \Delta OD) / \sigma_{e-h} L \approx 1.6 \times 10^{19}$  cm<sup>-3</sup>. Using the latter number and the estimated effective carrier mass  $m_{\text{opt}}^* \approx 0.125m_e$  (see below), we can calculate the plasma frequency  $\omega_p \approx 2\pi \times 100$  THz. Note that the different temporal dynamics of the measured absorption and phase changes suggest a time-dependent plasma frequency in the investigated temporal window.

The transient collision times calculated from the spectrally averaged phase shifts and absorption changes are presented in Fig. 4(a) for probe polarization parallel (red) and perpendicular (gray) relative to the polarization plane of the pump. The significant difference between both data sets might indicate that the Drude model is only partially applicable in the first 30 fs. In particular, the quantum kinetics responsible for the onset of collective behavior, such as Coulomb screening, which occurs within approximately one plasma oscillation period, lead to extremely efficient carrier-carrier interactions [10,21]. The subsequent relaxation of the hot electron-hole gas leads to a rise of the collision time from 3 fs to above 18 fs with a time constant of  $150 \pm 30$  fs [see black line in Fig. 4(a)].

Using the estimated carrier density of  $1.6 \times 10^{19}$  cm<sup>-3</sup> and the extracted transient scattering time, shown in Fig. 4(a), we used Eq. (2) to obtain the transient evolution of  $m_{\text{opt}}^*$  [see Fig. 4(b)]. For delay times  $t_d > 250$  fs the effective mass reaches an almost constant value of about  $0.125m_e$ . The latter value is in good agreement with the reported numbers for the

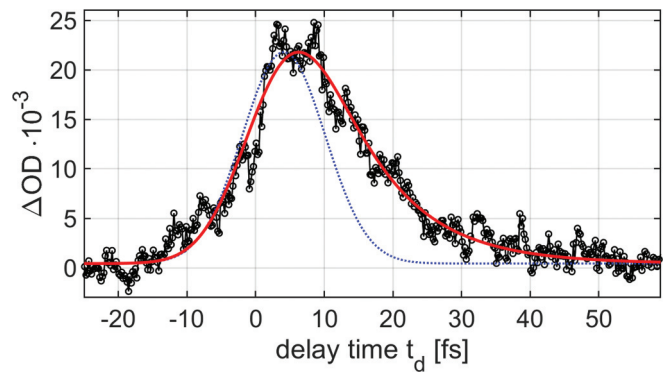


FIG. 5. Anisotropic (black) transient absorption changes averaged over the spectral range from  $1.39$  to  $1.81 \mu\text{m}$ . The blue dotted illustrates the instrument response function.

optical effective mass after thermalization of  $0.156$ – $0.168m_e$  [15]. The deviation is most probably due to the uncertainty in the used effective carrier absorption cross section. However, we emphasize that our main focus was on the temporal evolution of the extracted effective carrier mass. The data in Fig. 5(b) show a biexponential decay with faster decay time of 4 fs and slower time constant of  $58 \pm 5$  fs. Note that coherent interactions between pump and probe pulses could affect the faster time constant.

The carrier's effective mass depends very much on the averaged energy distribution in the bands [17]. The used internal pumping intensity  $\approx 0.17$  TW/cm<sup>2</sup> enables various excitation mechanisms as photon-assisted resonant absorption over the indirect gap, two-photon excitation over the zone-center direct gap, and even off-resonant interband tunneling [12]. The different excitation mechanisms generate electrons at various  $k$  points in the conduction band. Thus, the temporal evolution of the effective mass traces the averaged thermalization of the hot electron ensemble. Earlier studies [16,17] showed that the effective mass of hot carriers in Si exhibits an almost linear dependence on the carrier temperature. According to this, it can be expected that the carrier mass decay time of  $58 \pm 5$  fs represents the electron-phonon scattering time constant  $\tau_{e-ph}$ . The latter is in excellent agreement with the attosecond XUV transient absorption measurements under similar excitation conditions [12], where a time constant of 60 fs for electron-lattice dynamics was reported.

In contrast, Sato *et al.* [17] reported a nonlinear dependence of the Drude collision time on the carrier temperature, which suggests different time dependences of the collision time and the effective mass. Our experimental data provide the experimental verification of this theoretical prediction.

The anisotropic absorption change  $\Delta OD_{\text{aniso}} = (\Delta OD_{\parallel} - \Delta OD_{\perp})$  averaged over the spectral range from  $1.39$  to  $1.81 \mu\text{m}$  are presented in Fig. 5. The data indicate an extremely fast signal decay with a clear asymmetric temporal profile. The instrument response function of the setup (full width at half maximum of  $14 \pm 1$  fs) is shown for comparison. The anisotropic signal shows an additional exponential with decay time of  $10 \pm 2$  fs (red line in Fig. 5). The observation indicates that the optical excitation with few-cycle pulses leads to an asymmetric population of the Si conduction

band [11]. The extracted time constant of 10 fs is in qualitative agreement with the recently reported numbers for single electron momentum relaxation [8,38]. The latter process characterizes the ultrafast electron-electron interactions, which are responsible for the Coulomb screening and the onset of the collective electron-hole plasma properties [10,21]. The agreement of the anisotropy decay time with the oscillation period of the plasma frequency ( $\sim 100$  THz) supports the developed physical picture. Moreover, the fast anisotropy decay is in excellent agreement with plasma oscillation period, which characterizes the Coulomb screening and the onset of collective behavior of the electron-hole plasma [10].

In conclusion, we used a phase-resolved transient absorption spectroscopy with few-cycle pulses to study the relaxation dynamics of highly energetic (hot) carriers in silicon (100). The simultaneous detection of refraction and absorption changes following the strong field sub-5 fs excitation

is a powerful means for getting comprehensive information on the subsequent scattering dynamics. We applied the Drude model to extract the temporal evolutions of the carrier's collision time and effective mass. The latter decrease with time constants of 58 fs from 0.3 to about 0.125 due to thermalization of the hot electron-hole gas. The extracted collision time increases from 3 fs to above 18 fs with a time constant of  $150 \pm 30$  fs. The measured polarization resolved absorption data reveal an ultrafast single electron momentum relaxation time of 10 fs. We emphasize that detailed information on the hot electron transport properties is crucial for the applications in photovoltaic devices and next generation nano- and optoelectronics.

The authors acknowledge the financial support from the German Excellence Initiative via the Cluster of Excellence "e-Conversion" EXC 2089/1 – 390776260.

- 
- [1] E. Pop, Energy dissipation and transport in nanoscale devices, *Nano Res.* **3**, 147 (2010).
- [2] D. König, K. Casalenuovo, Y. Takeda, G. Conibeer, J. F. Guillemoles, R. Patterson, L. M. Huang, and M. A. Green, Hot carrier solar cells: Principles, materials and design, *Physica E* **42**, 2862 (2010).
- [3] R. T. Ross and A. J. Nozik, Efficiency of hot-carrier solar energy converters, *J. Appl. Phys.* **53**, 3813 (1982).
- [4] S. Kahmann and M. A. Loi, Hot carrier solar cells and the potential of perovskites for breaking the Shockley–Queisser limit, *J. Mater. Chem. C* **7**, 2471 (2019).
- [5] A. J. Minnich, M. S. Dresselhaus, Z. F. Ren, and G. Chen, Bulk nanostructured thermoelectric materials: Current research and future prospects, *Energy Environ. Sci.* **2**, 466 (2009).
- [6] F. Deschler, D. Neher, and L. Schmidt-Mende, Perovskite semiconductors for next generation optoelectronic applications, *APL Materials* **7**, 080401 (2019).
- [7] T. Ichibayashi, S. Tanaka, J. Kanasaki, K. Tanimura, and T. Fauster, Ultrafast relaxation of highly excited hot electrons in Si: Roles of the L-X intervalley scattering, *Phys. Rev. B* **84**, 235210 (2011).
- [8] H. Tanimura, J. Kanasaki, K. Tanimura, J. Sjakste, and N. Vast, Ultrafast relaxation dynamics of highly excited hot electrons in silicon, *Phys. Rev. B* **100**, 035201 (2019).
- [9] S. G. Engelbrecht, A. J. Reichel, and R. Kersting, Charge carrier relaxation and effective masses in silicon probed by terahertz spectroscopy, *J. Appl. Phys.* **112**, 123704 (2012).
- [10] R. Huber, F. Tauser, A. Brodschelm, M. Bichler, G. Abstreiter, and A. Leitenstorfer, How many-particle interactions develop after ultrafast excitation of an electron-hole plasma, *Nature (London)* **414**, 286 (2001).
- [11] M. Hase, M. Kitajima, A. M. Constantinescu, and H. Petek, The birth of a quasiparticle in silicon observed in time–frequency space, *Nature (London)* **426**, 51 (2003).
- [12] M. Schultze, K. Ramasesha, C. D. Pemmaraju, S. A. Sato, D. Whitmore, A. Gandman, J. S. Prell, L. J. Borja, D. Prendergast, and K. Yabana, Attosecond band-gap dynamics in silicon, *Science* **346**, 1348 (2014).
- [13] F. Schlaepfer, M. Lucchini, S. A. Sato, M. Volkov, L. Kasmi, N. Hartmann, A. Rubio, L. Gallmann, and U. Keller, Attosecond optical-field-enhanced carrier injection into the GaAs conduction band, *Nat. Phys.* **14**, 560 (2018).
- [14] S. K. Cushing, M. Zürich, P. M. Kraus, L. M. Carneiro, A. Lee, H.-T. Chang, C. J. Kaplan, and S. R. Leone, Hot phonon and carrier relaxation in Si(100) determined by transient extreme ultraviolet spectroscopy, *Struct. Dynam.* **5**, 054302 (2018).
- [15] D. M. Riffe, Temperature dependence of silicon carrier effective masses with application to femtosecond reflectivity measurements, *J. Opt. Soc. Am. B* **19**, 1092 (2002).
- [16] A. J. Sabbah and D. M. Riffe, Femtosecond pump-probe reflectivity study of silicon carrier dynamics, *Phys. Rev. B* **66**, 165217 (2002).
- [17] S. A. Sato, Y. Shinohara, T. Otobe, and K. Yabana, Dielectric response of laser-excited silicon at finite electron temperature, *Phys. Rev. B* **90**, 174303 (2014).
- [18] K. Sokolowski-Tinten and D. von der Linde, Generation of dense electron-hole plasmas in silicon, *Phys. Rev. B* **61**, 2643 (2000).
- [19] A. Leitenstorfer, C. Fürst, A. Laubereau, W. Kaiser, G. Tränkle, and G. Weimann, Femtosecond Carrier Dynamics in GaAs Far from Equilibrium, *Phys. Rev. Lett.* **76**, 1545 (1996).
- [20] C. Fürst, A. Leitenstorfer, A. Laubereau, and R. Zimmermann, Quantum Kinetic Electron-Phonon Interaction in GaAs: Energy Nonconserving Scattering Events and Memory Effects, *Phys. Rev. Lett.* **78**, 3733 (1997).
- [21] R. Huber, C. Kübler, S. Tübel, A. Leitenstorfer, Q. T. Vu, H. Haug, F. Köhler, and M.-C. Amann, Femtosecond Formation of Coupled Phonon-Plasmon Modes in InP: Ultrabroadband THz Experiment and Quantum Kinetic Theory, *Phys. Rev. Lett.* **94**, 027401 (2005).
- [22] B. Wang, J. Ryu, S. Choi, X. Zhang, D. Pribat, X. Li, L. Zhi, S. Park, and R. S. Ruoff, Ultrafast-charging silicon-based coral-like network anodes for lithium-ion batteries with high energy and power densities, *ACS Nano* **13**, 2307 (2019).
- [23] R. Dubé-Demers, S. LaRochelle, and W. Shi, Ultrafast pulse-amplitude modulation with a femtojoule silicon photonic modulator, *Optica* **3**, 622 (2016).

- [24] C. Karnetzky, P. Zimmermann, C. Trummer, C. Duque Sierra, M. Wörle, R. Kienberger, and A. Holleitner, Towards femtosecond on-chip electronics based on plasmonic hot electron nano-emitters, *Nat. Commun.* **9**, 2471 (2018).
- [25] F. Krausz and M. I. Stockman, Attosecond metrology: From electron capture to future signal processing, *Nat. Photon* **8**, 205 (2014).
- [26] K. Hütten, M. Mittermair, S. O. Stock, R. Beerwerth, V. Shirvanyan, J. Riemensberger, A. Duensing, R. Heider, M. S. Wagner, A. Guggenmos, S. Fritzsche, N. M. Kabachnik, R. Kienberger, and B. Bernhardt, Ultrafast quantum control of ionization dynamics in krypton, *Nat. Commun.* **9**, 719 (2018).
- [27] M. Uiberacker, T. Uphues, M. Schultze, A. J. Verhoef, V. Yakovlev, M. F. Kling, J. Rauschenberger, N. M. Kabachnik, H. Schröder, M. Lezius, K. L. Kompa, H.-G. Müller, M. J. J. Vrakking, S. Hendel, U. Kleineberg, U. Heinzmann, M. Drescher, and F. Krausz, Attosecond real-time observation of electron tunnelling in atoms, *Nature (London)* **446**, 627 (2007).
- [28] H. Fattahi, A. Schwarz, S. Keiber, and N. Karpowicz, Efficient, octave-spanning difference-frequency generation using few-cycle pulses in simple collinear geometry, *Opt. Lett.* **38**, 4216 (2013).
- [29] See Supplemental Material at <http://link.aps.org/supplemental/10.1103/PhysRevB.104.L041201> for a detailed description of the experimental setup, simulated wavelength-dependent Fabry-Pérot interferometer transmission/absorption, the experimental transient absorption in a 2-mm thick sample and the data shown in Figs. 2 and 3 averaged over one-oscillation period. It also includes Refs. [26–28].
- [30] K. Minoshima, M. Taiji, and T. Kobayashi, Femtosecond time-resolved interferometry for the determination of complex nonlinear susceptibility, *Opt. Lett.* **16**, 1683 (1991).
- [31] L. Lepetit, G. Chériaux, and M. Joffe, Linear techniques of phase measurement by femtosecond spectral interferometry for applications in spectroscopy, *J. Opt. Soc. Am. B* **12**, 2467 (1995).
- [32] G. Hernandez, *Fabry-Perot Interferometers* (Cambridge University Press, Cambridge, 1988).
- [33] M. C. Downer and C. V. Shank, Ultrafast Heating of Silicon on Sapphire by Femtosecond Optical Pulses, *Phys. Rev. Lett.* **56**, 761 (1986).
- [34] K. P. H. Lui and F. A. Hegmann, Ultrafast carrier relaxation in radiation-damaged silicon on sapphire studied by optical-pump–terahertz-probe experiments, *Appl. Phys. Lett.* **78**, 3478 (2001).
- [35] R. P. Prasankumar, A. Scopatz, D. J. Hilton, A. J. Taylor, R. D. Averitt, J. M. Zide, and A. C. Gossard, Carrier dynamics in self-assembled ErAs nanoislands embedded in GaAs measured by optical-pump terahertz-probe spectroscopy, *Appl. Phys. Lett.* **86**, 201107 (2005).
- [36] C. A. Schmuttenmaer, Exploring dynamics in the far-infrared with terahertz spectroscopy, *Chem. Rev.* **104**, 1759 (2004).
- [37] D. K. Schroder, R. N. Thomas, and J. C. Swartz, Free carrier absorption in silicon, *IEEE J. Solid-State Circuits* **13**, 180 (1978).
- [38] M. Bernardi, D. Vigil-Fowler, J. Lischner, J. B. Neaton, and S. G. Louie, *Ab Initio* Study of Hot Carriers in the First Picosecond after Sunlight Absorption in Silicon, *Phys. Rev. Lett.* **112**, 257402 (2014).